

# Emergence of epithelial cell density waves

Shunsuke Yabunaka<sup>1\*</sup> and Philippe Marcq<sup>2†</sup>

<sup>1</sup> *Fukui Institute for Fundamental Chemistry, Kyoto University, Kyoto, Japan and*

<sup>2</sup> *Laboratoire Physico Chimie Curie, Institut Curie, Université Marie et Pierre Curie, CNRS UMR 168, 26 rue d'Ulm, F-75248 Paris Cedex 05, France*

(Dated: August 22, 2017)

Epithelial cell monolayers exhibit traveling mechanical waves. We rationalize this observation thanks to a hydrodynamic description of the monolayer as a compressible, active and polar material. We show that propagating waves of the cell density, polarity, velocity and stress fields may be due to a Hopf bifurcation occurring above threshold values of active coupling coefficients.

## I. INTRODUCTION

Pattern-forming instabilities [1] play a pivotal role in the morphogenesis and spatio-temporal organization of living organisms. Paradigmatic examples include the morphogen patterns of developing embryos [2] and the cooperative behaviour of large assemblies of microorganisms [3], for instance in bacterial colonies. Nonlinear oscillators contribute to our understanding of phenomena as diverse as genetic clocks [4] or calcium signaling [5]. Most processes occurring at the scale of a single cell are strongly dissipative and driven by the consumption of chemical fuel. A recognition of this basic fact has led in the past few decades to a strong cross-fertilization of concepts and methods between non-equilibrium physics and cell biology [6, 7].

At the scale of the tissue, Serra-Picamal *et al.* [8] discovered that the expansion into free space of Madin-Darby canine kidney (MDCK) epithelial cell monolayers is accompanied by traveling mechanical waves of the velocity, strain rate, traction force and stress fields. This observation has since been confirmed independently by others, in the same geometry [9, 10], as well as in confined domains [11]. To the best of our knowledge, the biological function of the epithelial waves remains unknown. *In vitro* epithelial cell monolayers are a robust model system for epithelial tissues, amenable to controlled experiments in various geometries and conditions [12–15]. Monolayer expansion has been studied theoretically by several authors [16–19], and shown to be conducive to spatio-temporally disordered dynamical regimes [20, 21]. The first theoretical account of the mechanical waves given in [8] necessitated a nonlinear cell rheology. More recent models involve either a linear elastic [10, 11, 22] or a viscous [23] rheology, as well as couplings of the mechanical stress to additional fields such as the myosin density [11, 22] or the cell polarity [10, 23]. Although traveling waves of the cell density field have been observed during epithelial spreading [10], the evolution equation of the cell density has not been included in existing models. This is all the more surprising that the cell density field

of epithelial cell monolayers is known to fluctuate in both time and space, both *in vitro* [24, 25] and *in vivo* [26]: the corresponding epithelial flows are thus *compressible*.

In this work, we formulate and justify a minimal physical model of a cohesive tissue able to sustain traveling mechanical waves. Noting that the waves occur in the absence of cell division [9], we defer a rigorous treatment of cell proliferation to a separate work [27] and treat the cell density field as a conserved quantity. Importantly, waves are suppressed by inhibitors of contractility, such as blebbistatin [8]. We therefore consider tissue activity as a necessary ingredient. Experiments have shown that inhibitors of polarity also suppress the waves [10]: as a consequence we include tissue polarity in our description. Within the framework of linear nonequilibrium thermodynamics [28], we write the constitutive equations for a one-dimensional, compressible, polar and active material, including lowest-order nonlinear active terms [29, 30] that involve the cell density field. We show that Hopf bifurcations occur beyond threshold values of active parameters, leading to traveling waves for the relevant mechanical fields (cell density, velocity and polarity), and thus also for the tissue traction force and stress fields. Inhibition assays of active and polar behaviour are mimicked by numerical simulations of our model equations. We compare our minimal model with competing formulations, and discuss the robustness of our findings to the inclusion of additional terms.

## II. MODEL

Since relevant experiments were performed in a quasi-one-dimensional geometry [8, 9, 11], we focus on the one dimensional case. We enforce periodic boundary conditions in a system of constant spatial extension  $L$ , with space coordinate  $x$  and time  $t$ .

### A. Conservation equations

The conservation equation for cell number reads:

$$\partial_t \rho + \partial_x (\rho v) = 0, \quad (1)$$

\* yabunaka@scphys.kyoto-u.ac.jp

† philippe.marcq@curie.fr

where  $\rho(x, t)$  and  $v(x, t)$  respectively denote the cell number density and velocity fields. Denoting  $\sigma(x, t)$  the (internal) tissue stress field and  $t^{ext}(x, t)$  the (external) force exerted by the substrate on the tissue, the conservation of linear momentum is expressed as:

$$\partial_x \sigma = -t^{ext}. \quad (2)$$

Motile cells within the tissue are polar, with a well-defined front and rear: coarse-graining over a suitable mesoscopic scale the cell polarity yields the tissue polarity field  $p(x, t)$ . The external force is assumed to be due both to fluid friction, with a friction coefficient  $\xi$ , and to active motility forces oriented along the polarity  $p(x, t)$ , with an amplitude  $t_a$  [10, 11, 22, 23]:

$$t^{ext} = -\xi v + t_a p. \quad (3)$$

### B. Thermodynamics

Including the spatial gradients of the cell density and polarity fields, we assume that the total free energy of the cell monolayer reads

$$F = \int dx f(\rho, \partial_x \rho, \partial_x^2 \rho, p, \partial_x p, \partial_x^2 p),$$

where integration is performed over the domain of size  $L$ , and  $f$  is the free energy density. Here and below a dot denotes the total derivative, as in  $\dot{f} = \partial_t f + v \partial_x f$ . We evaluate the free energy variation rate

$$\dot{F} = \frac{d}{dt} \int dx f = \int dx \partial_t f = \int dx (\dot{f} - v \partial_x f) = \int dx (\dot{f} + f \partial_x v)$$

following an integration by parts. The chain rule yields

$$\begin{aligned} \dot{f} = & \frac{d\rho}{dt} \frac{\partial f}{\partial \rho} + \frac{d}{dt} (\partial_x \rho) \frac{\partial f}{\partial (\partial_x \rho)} + \frac{d}{dt} (\partial_x^2 \rho) \frac{\partial f}{\partial (\partial_x^2 \rho)} \\ & + \frac{dp}{dt} \frac{\partial f}{\partial p} + \frac{d}{dt} (\partial_x p) \frac{\partial f}{\partial (\partial_x p)} + \frac{d}{dt} (\partial_x^2 p) \frac{\partial f}{\partial (\partial_x^2 p)}. \end{aligned}$$

Using (3), and the periodic boundary conditions, the power of external forces done on the monolayer reads

$$\Pi = \int dx v (-\xi v + t_a p) = - \int dx v \partial_x \sigma = \int dx \sigma \partial_x v.$$

For isothermal transformations at temperature  $T$ , we obtain

$$T\Sigma = \Pi - \dot{F} + \int dx r \Delta\mu,$$

where  $\Sigma$  denotes the entropy production rate, and we included an additional (chemical) active term [29], with  $r$  and  $\Delta\mu$  respectively the reaction rate and chemical potential difference of nucleotide hydrolysis. Following [29, 30], we lump under the term “activity” all cell pro-

cesses driven by nucleotide hydrolysis, which are relevant for cell and tissue mechanics. This includes motor-driven contractility as well as actin polymerization.

Noting that

$$\begin{aligned} \frac{d}{dt} (\partial_x p) &= \partial_x \frac{dp}{dt} - (\partial_x p)(\partial_x v) \\ \frac{d}{dt} (\partial_x^2 p) &= \partial_x^2 \frac{dp}{dt} - (\partial_x p)(\partial_x^2 v) - 2(\partial_x^2 p)(\partial_x v) \end{aligned}$$

(and analogous equations concerning the density field), integrations by part yield

$$T\Sigma = \int dx ((\sigma + \pi) \partial_x v + \dot{p} h + r \Delta\mu), \quad (4)$$

with the following definitions of the molecular field  $h$ , conjugate to the polarity:

$$h = -\frac{\partial f}{\partial p} + \partial_x \left( \frac{\partial f}{\partial (\partial_x p)} \right) - \partial_x^2 \left( \frac{\partial f}{\partial (\partial_x^2 p)} \right), \quad (5)$$

and of the pressure  $\pi$ , conjugate to the density

$$\begin{aligned} \pi = & -f + \rho \left[ \frac{\partial f}{\partial \rho} - \partial_x \left( \frac{\partial f}{\partial (\partial_x \rho)} \right) + \partial_x^2 \left( \frac{\partial f}{\partial (\partial_x^2 \rho)} \right) \right] \\ & + (\partial_x \rho) \left[ \frac{\partial f}{\partial (\partial_x \rho)} - \partial_x \left( \frac{\partial f}{\partial (\partial_x^2 \rho)} \right) \right] + (\partial_x^2 \rho) \frac{\partial f}{\partial (\partial_x^2 \rho)} \\ & + (\partial_x p) \left[ \frac{\partial f}{\partial (\partial_x p)} - \partial_x \left( \frac{\partial f}{\partial (\partial_x^2 p)} \right) \right] + (\partial_x^2 p) \frac{\partial f}{\partial (\partial_x^2 p)}. \end{aligned} \quad (6)$$

### C. Constitutive equations

From (4), we identify the following conjugate flux-force pairs

$$\begin{aligned} & \text{Flux} \leftrightarrow \text{Force} \\ & \sigma + \pi \leftrightarrow \partial_x v \\ & \dot{p} \leftrightarrow h \\ & r \leftrightarrow \Delta\mu. \end{aligned}$$

Following a standard procedure, the constitutive equations read

$$\sigma + \pi = \eta \partial_x v + \sigma_a + \gamma_a \rho \quad (7)$$

$$\dot{p} = \Gamma_p h - \lambda p \partial_x v - \alpha_a p \partial_x p + \delta_a \partial_x \rho \quad (8)$$

omitting the equation expressing as a function of thermodynamic forces the field  $r$ . The dynamic viscosity  $\eta$  and the kinetic coefficient  $\Gamma_p$  are positive. We include lowest-order (nonlinear) active coupling coefficients, denoted by the index  $a$ , and proportional to  $\Delta\mu$ , as in  $\gamma_a = \gamma \Delta\mu$ . A contractile material is characterized by a positive active stress  $\sigma_a$ , which may ensure, for large enough positive values, that the cell monolayer is everywhere under tension, as observed experimentally [8]. Since  $r$  may be propor-

tional to density, active coupling coefficients may also be proportional to  $\rho$ . This justifies the active term  $\gamma_a \rho$  in (7). The invariance properties of polar media allow for an active coupling between polarity and density gradient, with a coefficient  $\delta_a$  in (8). Two advection terms with coupling coefficients  $\alpha_a$  and  $\lambda$ , of arbitrary signs, are included in Eq. (8), in agreement with earlier studies of active liquid crystals [31].

#### D. Free energy density

In our minimal description, we define the free energy density as

$$f = \psi_\rho(\rho) + \varphi_p(p) + \frac{\nu}{2} (\partial_x^2 \rho)^2 \quad (9)$$

(see Sec. V A for possible additional terms). The functions  $\psi_\rho(\rho)$  and  $\varphi_p(p)$  depend respectively on density and polarity only. We include a stabilizing ( $\nu \geq 0$ ) higher-order density gradient term  $\frac{\nu}{2} (\partial_x^2 \rho)^2$ . It is akin to the higher-order displacement gradient terms used in second gradient elasticity [32, 33]. We obtain the conjugate fields from (5-6):

$$h = -\varphi'_p(p) \quad (10)$$

$$\pi = -f + \rho [\psi'_\rho(\rho) + \nu \partial_x^4 \rho] + \nu [(\partial_x^2 \rho)^2 - (\partial_x \rho) (\partial_x^3 \rho)] \quad (11)$$

In the following, we expand the free energy density  $f$  in the vicinity of a state characterized by a finite polarity  $p_0$  and a finite density  $\rho_e$ . We thus define

$$\varphi_p(p) = -\frac{a_2}{2} p^2 + \frac{a_4}{4} p^4, \quad (12)$$

where  $a_2, a_4$  are positive coefficients and

$$\psi_\rho(\rho) = \frac{1}{2K} \left( \frac{\rho - \rho_e}{\rho_e} \right)^2 + \frac{1}{4K_4} \left( \frac{\rho - \rho_e}{\rho_e} \right)^4, \quad (13)$$

where  $K \geq 0$  is the compressibility modulus, and  $\rho_e$  is a reference density. The quartic term, with coefficient  $K_4 \geq 0$ , is included for numerical stability. It makes the density-dependent potential steeper, but does not alter the linear stability analysis.

#### E. Summary

To summarize Eqs. (1-3) and (7-8), the dynamics is governed by a set of three coupled partial differential equations, with periodic boundary conditions on all fields:

$$\partial_t \rho + \partial_x (\rho v) = 0 \quad (14)$$

$$-\partial_x \pi + \eta \partial_x^2 v + \gamma_a \partial_x \rho = \xi v - t_a p \quad (15)$$

$$\partial_t p + v \partial_x p + \lambda p \partial_x v + \alpha_a p \partial_x p = \Gamma_p h + \delta_a \partial_x \rho \quad (16)$$

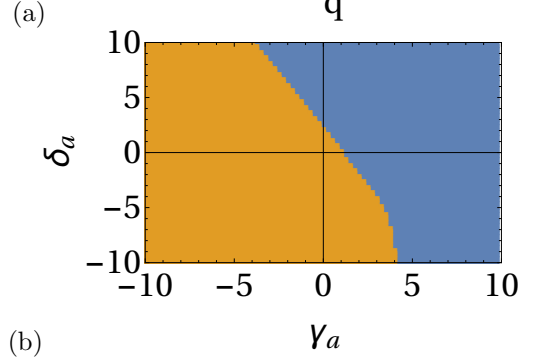
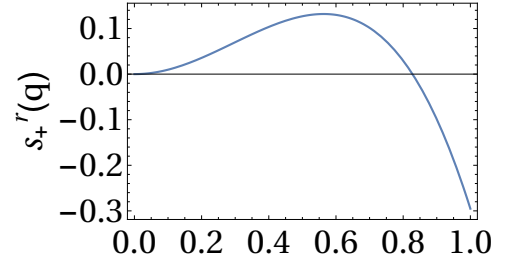


FIG. 1. **Linear stability analysis.** (a) Plot of the real part of the largest growth rate  $s_+^r(q)$  as a function of wave number  $q$ . All parameters are set equal to 1 (including  $\gamma_a$  and  $\delta_a$ ), except  $p_0 = 0.5$ ,  $\xi = 0.5$ . We find  $q_{\max} = \arg\max_q(s_+^r(q)) = 0.56$ , with a wave velocity  $c = s_+^i(q_{\max})/q_{\max} = 1.07$  greater than the mean tissue velocity  $v_0 = t_a p_0 / \xi = 1$ . We checked that  $s_-^r(q) < 0, \forall q$ . (b) Bifurcation diagram in the  $(\gamma_a, \delta_a)$  plane. The yellow (*resp.* blue) domain corresponds to a stable (*resp.* unstable) homogeneous state.

where  $h$  and  $\pi$  are defined by (10) and (11) respectively.

### III. LINEAR STABILITY ANALYSIS

The system (14-16), supplemented with (10-11) and (12-13) admits stationary, homogeneous solutions

$$(\rho, p, v) = (\rho_0, p_0, v_0)$$

with finite polarity  $p_0 = \sqrt{a_2/a_4}$ , finite velocity  $v_0 = t_a p_0 / \xi$ , and arbitrary  $\rho_0$ . For simplicity, we set  $\rho_0 = \rho_e$  in the following.

We study the growth rate  $s$  of perturbations of wave number  $q$ :

$$(\rho, p, v) = (\rho_e, p_0, v_0) + (\delta\rho, \delta p, \delta v) e^{st - iqx}. \quad (17)$$

Substituting (17) into (14-16) with (10-11) and (12-13), we obtain to linear order a set of coupled equations, written in matrix form

$$\mathcal{L} \begin{pmatrix} \delta\rho \\ \delta p \\ \delta v \end{pmatrix} = \begin{pmatrix} 0 \\ 0 \\ 0 \end{pmatrix} \quad (18)$$

with

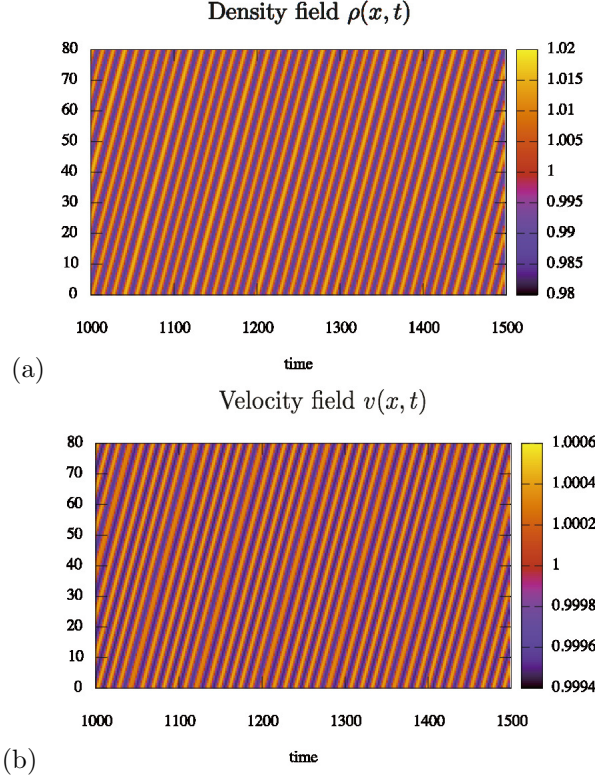


FIG. 2. **A traveling wave:** all parameters are set equal to one  $K = \rho_e = a_2 = \eta = \lambda = \Gamma_p = t_a = \alpha_a = \delta_a = \gamma_a = 1$ , except for  $\xi = p_0 = 0.5$  and  $K_4 = 0.0005$ . The cell density (a) and velocity (b) kymographs are presented when  $t \geq 1000$ , after transients have died out. The polarity and stress fields also exhibit stable traveling wave solutions for the same parameter values (not shown).

$$\mathcal{L} = \begin{pmatrix} s - iqv_0 & 0 & -iq\rho_e \\ iq\left(\frac{1}{K\rho_e} - \gamma_a + \nu\rho_e q^4\right) & t_a & -(\xi + \eta q^2) \\ iq\delta_a & s + 2a_2\Gamma_p - iq(v_0 + \alpha_a p_0) & -iq\lambda p_0 \end{pmatrix}$$

whose solution yields the wavenumber dependence of the complex-valued growth rates  $s_{\pm}(q) = s_{\pm}^r(q) + is_{\pm}^i(q)$ . A Hopf bifurcation occurs above a threshold value of a control parameter where the real part of the growth rate  $s_{+}^r$  becomes positive, while its imaginary part is non-zero  $s_{+}^i \neq 0$ . For parameter values above threshold, the velocity of traveling waves is given by  $c = s_{+}^i(q_{\max})/q_{\max}$ , where  $q_{\max}$  is the most unstable wavenumber  $q_{\max} = \text{argmax}_q(s_{+}^r(q))$ .

We performed numerically the linear stability analysis. In Fig. 1a, we plot  $s_{+}^r(q)$  with all parameter values set equal to one ( $t_a = \eta = \Gamma_p = \lambda = K = \rho_e = \alpha_a = \delta_a =$

$\gamma_a = 1$ ), except  $\xi = p_0 = 0.5$ , and find that traveling waves are expected in this system, with a wave propagation velocity equal to  $c = c(q_{\max}) = 1.07$ , larger than the average velocity of the flow  $v_0 = 1$ . In Fig. 1b, we plot the bifurcation diagram in the  $(\gamma_a, \delta_a)$  plane: a Hopf bifurcation occurs for large enough values of these active parameters.

From Eqs. (2-3), we deduce

$$-iq\delta\sigma = \xi\delta v - t_a\delta p,$$

where the first term on the right hand side is dissipa-

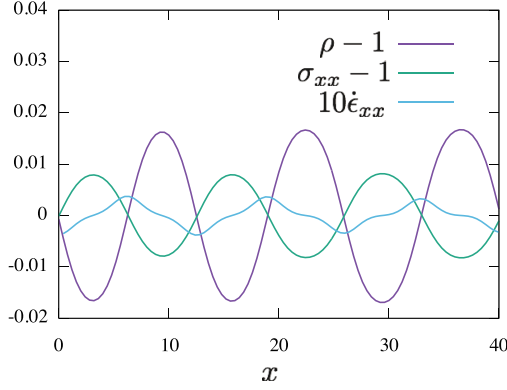


FIG. 3. **Spatial profiles** of the density, stress and strain rate fields at  $t = 1000$ . Parameter values are as in Fig. 2.

tive. Eliminating  $\delta\rho$  from (18), we find that, in the linear regime,  $\delta p = (g^r(q) + ig^i(q))\delta v$ , where  $g^r$  and  $g^i$  are real functions of the wavenumber, and obtain by substitution

$$-iq\delta\sigma = ((\xi - t_a g^r(q)) - it_a g^i(q))\delta v.$$

The presence of an imaginary contribution  $it_a g^i(q)$  may explain the apparently “elastic” behaviour of the mechanical waves as presented in [8], while being in fact due to the active and polar nature of this compressible, viscous material (see a similar discussion in [23]).

#### IV. NUMERICAL SIMULATIONS

In this section, we present the results of numerical simulations of Eqs. (14-16), supplemented with (10-13). As an initial condition, we take the uniform state with  $\rho = \rho_e$ ,  $p = p_0$ ,  $v = v_0 = t_a p_0 / \xi$  and add a noise of small amplitude. We used a finite-difference method and integrated Eqs. (14-16) on a discretized 1d space with mesh size  $\Delta x = 0.01$  and time step  $\Delta t = 0.0001$  as follows: Given the density field  $\rho(x, t)$  and the polarity field  $p(x, t)$  at a time step  $t$ , we solve Eq. (15) for the velocity field  $v(x, t)$ . Next, using Eq. (14) and Eq. (16), we determine the density field  $\rho(x, t + \Delta t)$  and the polarity field  $p(x, t + \Delta t)$  at the next time step  $t + \Delta t$  with the explicit Euler method.

In Fig. 2, we set all parameters to one ( $K = \rho_e = a_2 = \eta = \lambda = \Gamma_p = \gamma_a = t_a = \alpha_a = \delta_a = 1$ ) except for  $\xi = p_0 = 0.5$  and  $K_4 = 0.0005$ . As predicted by the linear stability analysis in the previous section, we confirm numerically that the instability occurs and the propagation velocity ( $c \sim 1.07$ ) is slightly larger than the mean tissue velocity  $v_0 = t_a p_0 / \xi = 1$ . The transient time scale is of the order of  $10^2$ . In Fig. 3, we show for the same parameter values the spatial profiles of the cell density, stress and strain rate  $\dot{\epsilon}_{xx} = \partial_x v(x, t)$  at  $t = 1000$ . The stress and strain rate are out-of-phase, while the stress and the cell density are in antiphase. If we consider that the cell area measured experimentally corresponds to the

inverse of the cell density, both phase relations agree with experimental observations, which have been interpreted as evidence for an elastic rheology [8]. However, our constitutive equation (7) is that of a compressible, viscous material, also endowed with active and polar properties.

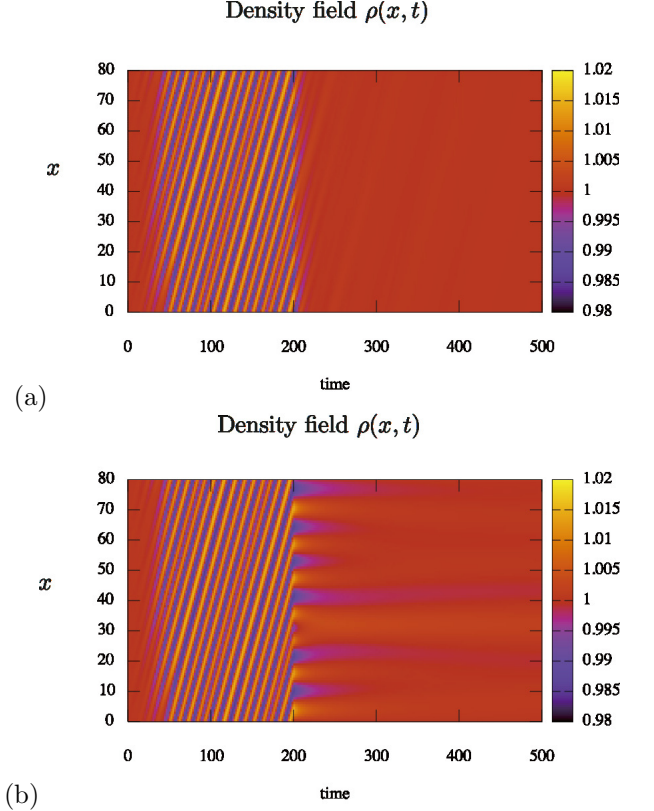


FIG. 4. **Numerical experiments mimicking inhibition assays:** density kymographs, with parameters as in Fig. 2 until  $t = 200$ . (a) Experimental inhibition of contractility by blebbistatin is mimicked by lowering the active parameters  $\delta_a$  and  $\gamma_a$  to 0.5 when  $t \geq 200$ . (b) Experimental inhibition of Arp 2/3 is mimicked by lowering  $p_0$  to a large negative value  $-500$  when  $t \geq 200$ . In both cases the traveling wave pattern disappears when  $t \geq 200$ , as predicted by linear stability analysis.

Numerical simulations allow to mimic inhibition assays by tuning the value(s) of parameter(s) that would be changed due to the application of a drug. When we lower the value of the active parameters to  $\delta_a = 0.5$ ,  $\gamma_a = 0.5$  at  $t = 200$ , we observe that the traveling wave rapidly disappears (see Fig. 4a), as observed experimentally when inhibiting contractility. In a similar manner, when we change the reference polarity value from a finite  $p_0$  to  $p_0 = 0$  (by setting  $a_2 = -500$  at  $t = 200$ ), the traveling waves also disappears quickly (see Fig. 4b), as observed experimentally when inhibiting Arp 2/3.

Finally, Fig. 5 shows an example of a traveling wave observed farther from threshold, with  $\alpha_a = 2$ ,  $\gamma_a = \delta_a = 3$ , and other parameters as in Fig. 2. The propagation velocity is accordingly larger  $c \sim 1.3$ .

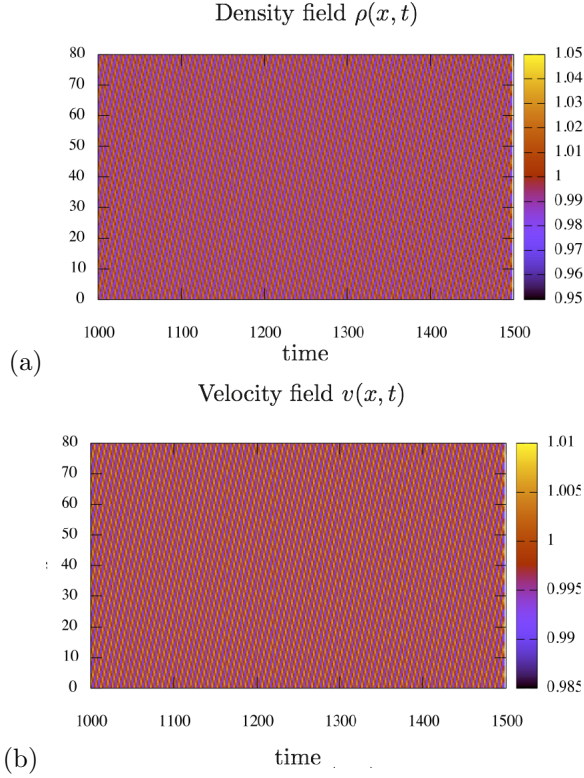


FIG. 5. **A traveling wave:** Parameters are as in Fig. 2, except the active parameters  $\alpha_a = 2$ ,  $\gamma_a = \delta_a = 3$ . Kymographs of (a) the cell density (a); and (b) the velocity field are presented when  $t \geq 1000$ , after transients have died out. The polarity and stress fields also exhibit stable traveling wave solutions for the same parameter values (not shown).

## V. DISCUSSION

### A. Robustness

Additional terms also invariant under simultaneous inversion of space and polarity are allowed by symmetry in the definition of the free energy density (9). A more complete, but also more complex expression of the free energy density as an expansion in terms of cell density, polarity, and their gradients reads

$$f = \psi_\rho(\rho) + \frac{K_\rho}{2} (\partial_x \rho)^2 + \frac{\nu}{2} (\partial_x^2 \rho)^2 + \varphi_p(p) + \frac{K_F}{2} (\partial_x p)^2 + \frac{\nu_K}{2} (\partial_x^2 p)^2 + w_1 \partial_x p + w_2 \rho \partial_x p + w_3 p \partial_x \rho + w_4 \partial_x \rho \partial_x^2 p + w_5 \partial_x p \partial_x^2 \rho + \dots,$$

and is by no means exhaustive. It leads to more complex expressions of the conjugate fields  $\pi$  and  $h$ . Here  $K_F \geq 0$  is Frank's constant, the parameter  $\nu_K \geq 0$  controls a term that further stabilizes large wavenumber modes, and the  $w_i$ 's couple density and polarity gradients. Note that the terms penalizing polarity gradients may become relevant in the presence of topological defects.

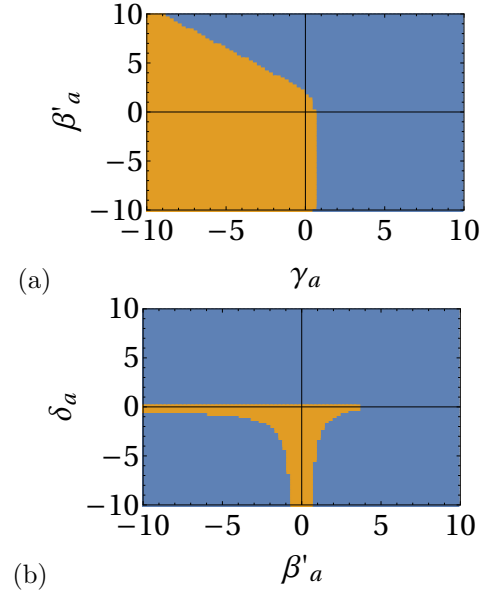


FIG. 6. **Bifurcation diagrams:** (a) in the  $(\gamma_a, \beta'_a)$  plane, with  $\delta_a = 1$ . (b) in the  $(\beta'_a, \delta_a)$  plane, with  $\gamma_a = 1$ . Our minimal model is supplemented with the  $\beta'_a p^2$  term in (19), while

other parameter values are as in Fig. 1b. The yellow (*resp.* blue) domain corresponds to a stable (*resp.* unstable) homogeneous state.

Similarly, additional nonlinear active terms could be included in the right hand side of (7):

$$\sigma = -\pi + \eta \partial_x v + \beta_a \partial_x p + \beta'_a p^2 + \sigma_a + \gamma_a \rho + \dots \quad (19)$$

and of (8):

$$\dot{p} = \Gamma_p h + a_a p + a'_a \rho p - \lambda p \partial_x v - \alpha_a p \partial_x p + \delta_a \partial_x \rho + \dots \quad (20)$$

since they also respect the invariance properties of  $\sigma$  and  $\dot{p}$ .

We checked that these additional terms, while making the model more complex, do not change our qualitative conclusions: activity-driven traveling waves occur in large regions of the parameter space that govern active polar media (see also [31, 34]). As an example motivated by [23], we add to our minimal model the  $\beta'_a p^2$  term in (19), and show in Fig. 6 the resulting bifurcation diagrams in the  $(\gamma_a, \beta'_a)$  plane, at constant  $\delta_a$  and in the  $(\beta'_a, \delta_a)$  plane, at constant  $\gamma_a$  (compare with Fig. 1b).

### B. Behaviour close to $p = 0$

When the free energy is expanded close to  $p = 0$ , bifurcations driven by the active parameters  $\gamma_a$  and  $\delta_a$  also occur. This case is obtained by setting  $a_2 < 0$  in (12), and leads to substituting  $p_0 \rightarrow 0$ ,  $v_0 \rightarrow 0$  in (18). However, we find this time that  $s_+^i(q_{\max}) = 0$ , *i.e.* that the bifurcation is stationary and lead to *standing waves*. This

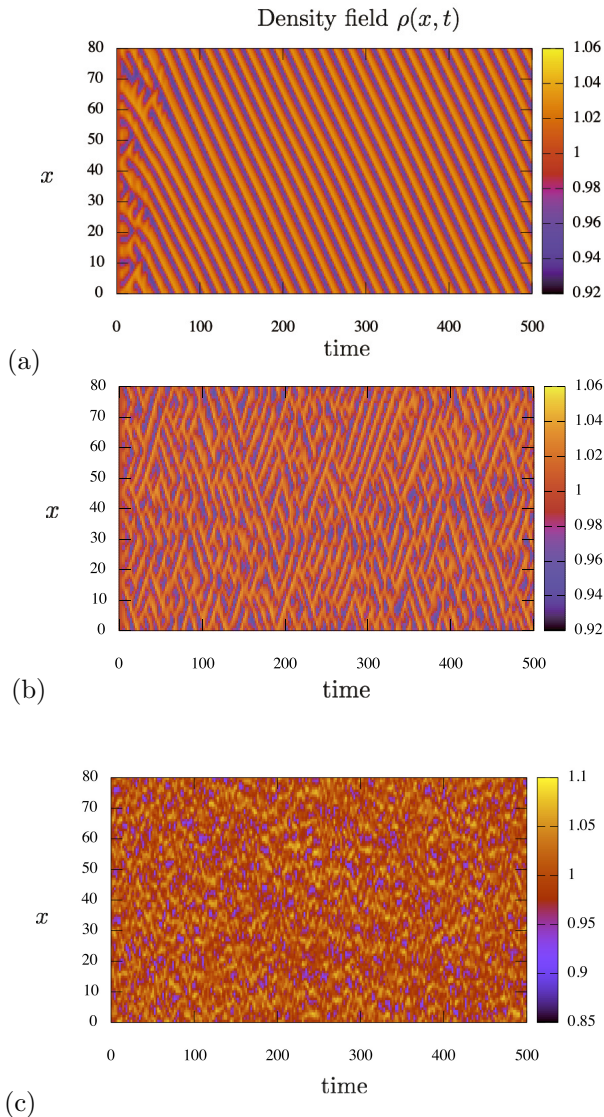


FIG. 7. **Secondary bifurcations.** Our minimal model is supplemented with the  $\beta'_a p^2$  term in (19), with parameters as in Fig. 2, except  $a_2 = -1$ ,  $\beta_a = 0.1$ ,  $\gamma_a$ ,  $\delta_a$  and  $\beta'_a$ . Since  $a_2 < 0$ , the primary bifurcation is stationary. Density kymographs are shown, with (a) a traveling wave:  $\gamma_a = 2$ ,  $\delta_a = 4$  and  $\beta'_a = 20$ ; (b) coexistence of rightwards and leftwards traveling waves:  $\gamma_a = 2$ ,  $\delta_a = 4$  and  $\beta'_a = 30$ ; (c) a disordered pattern:  $\gamma_a = 4$ ,  $\delta_a = 8$  and  $\beta'_a = 20$ .

is consistent with previous work on active polar materials [35], and leads us to expect that traveling waves may then arise farther from threshold due to secondary bifurcations.

As an example, we show in Fig. 7 that a secondary bifurcation occurs in the presence of  $\beta_a$  and  $\beta'_a$ : With the parameters  $a_2 = -1 < 0$ ,  $\gamma_a = 2$ ,  $\delta_a = 4$ ,  $\beta_a = 0.1$  and  $\beta'_a = 20$ , we found a travelling wave solution. When increasing  $\beta'_a$  and fixing the other parameters, we observed that the stationary periodic pattern becomes unstable for  $\beta'_a \gtrsim 11.5$ . We also obtained disordered patterns by fur-

ther increasing the active parameters. The cases shown in Fig. 7 should be considered as examples. A full investigation of the complex spatio-temporal patterns generated by our model is left for future study.

### C. Model comparison

A significant difference with the treatments proposed in [11, 22] is that we take into account the compressibility of the monolayer [24, 25] through the cell density balance equation (see [23] for an alternative way to treat incompressibility). Our formulation is more parsimonious than [11, 22] since we do not need to introduce an evolution equation for an additional chemical field in order to generate the instability. While the phenomenological model of wave generation proposed in [10] is based on a mechanotransduction pathway involving the protein Merlin [36], other authors favour the ERK Map kinase as a possible mechanochemical mediator [11]. Our approach does not depend upon a specific biochemical mechanism. It is based on general physical principles, notably symmetry arguments, which remain valid irrespective of the specific molecular mechanism at play. We propose a mechanism where activity couples to the cell density field. Only detailed comparison with experimental data is liable to determine which of the possible nonlinearities is involved.

Traveling waves are driven by either strong enough active stresses or strong enough active couplings in the evolution equation of the polarity field. As a consequence, their emergence does not depend on a specific rheology. Due to the 1D geometry, our choice of a rheology is somewhat ambiguous. According to Eq. (7), we assume that the epithelial rheology is that of a compressible, viscous fluid. Since it cancels at a finite value of the density, the pressure can also be interpreted in 1D as minus the elastic stress,  $\pi = -\sigma_{el}$ . From this viewpoint, the epithelium rather behaves as a viscoelastic solid. An elastic behaviour corresponds to the limit of zero viscosity. Setting  $\eta = 0$  only shifts the instability threshold without altering the structure of the bifurcation diagram. Thus traveling waves arise in our model for a viscous, an elastic, and a viscoelastic rheology (Kelvin model). We conjecture that the equations one would write for a viscoelastic liquid (Maxwell model) would also give rise to activity-driven traveling waves [35].

## VI. CONCLUSION

Within the framework of linear nonequilibrium thermodynamics, we wrote the constitutive equations for a one-dimensional, compressible, polar and active material, including lowest-order nonlinear active terms. We showed that Hopf bifurcations occur at threshold values of active parameters, leading to traveling waves for the relevant mechanical fields (density, velocity, polarity and stress). We thus formulated and justified a minimal,

physical model of a tissue able to sustain traveling mechanical waves. A lower value of active parameters may suppress the waves, in agreement with experimental observation following the application of a drug inhibiting contractility. Switching to a state without a preferred polarity may also suppress the waves, just as inhibiting Arp 2/3 does in the cell monolayer. Not all epithelial cell types self-organize to generate traveling waves [37]: in the light of our model, this suggests that active parameters are strongly cell-type dependent, and may accordingly be above or below the instability threshold.

In order to describe faithfully the experimental observations [8, 10], the model needs to be extended to a 2D geometry, and to include a moving free boundary in the numerical simulations, close to which polar order may be confined within a band of finite extension [19]. The same

epithelial monolayers exhibit topological defects of the cell shape tensor field characteristic of a *nematic* material [38]. A more complete theory should take into account both types of orientational order.

## ACKNOWLEDGEMENTS

We wish to thank Carles Blanch-Mercader, Estelle Gauquelin, François Graner, Shreyansh Jain, Benoit Ladoux and Sham Tlili for enlightening discussions and helpful suggestions. S.Y. was supported by Grant-in-Aid for Young Scientists a(B) (15K17737), Grants-in-Aid for Japan Society for the Promotion of Science (JSPS) Fellows (Grant No. 263111), and the JSPS Core-to-Core Program "Non-equilibrium dynamics of soft matter and information".

- 
- [1] M. C. Cross and P. C. Hohenberg, *Rev. Mod. Phys.*, 1993, **65**, 851–1112.
  - [2] H. Meinhardt, *Curr Top Dev Biol*, 2008, **81**, 1–63.
  - [3] E. ben Jacob, I. Cohen and H. Levine, *Adv. Physics*, 2000, **49**, 395 – 554.
  - [4] K. Kruse and D. Riveline, *Curr Top Dev Biol*, 2011, **95**, 67–91.
  - [5] M. Falcke, *Adv. Phys.*, 2003, **53**, 255–440.
  - [6] E. Karsenti, *Nat. Rev. Mol. Cell Biol.*, 2008, **9**, 255–262.
  - [7] C. Beta and K. Kruse, *Annu Rev Cond Matter Phys*, 2017, **8**, 239–264.
  - [8] X. Serra-Picamal, V. Conte, R. Vincent, E. Anon, D. T. Tambe, E. Bazellieres, J. P. Butler, J. J. Fredberg and X. Trepat, *Nat Phys*, 2012, **8**, 628–634.
  - [9] S. Tlili, *PhD thesis*, Université Paris Diderot, Paris, France, 2015.
  - [10] S. Tlili, E. Gauquelin, B. Li, O. Cardoso, B. Ladoux, H. Delanoë-Ayari and F. Graner, *arXiv:1610.05420*, 2016.
  - [11] J. Notbohm, S. Banerjee, K. Utuje, B. Gweon, H. Jang, Y. Park, J. Shin, J. Butler, J. Fredberg and M. Marchetti, *Biophys J*, 2016, **110**, 2729–2738.
  - [12] M. Poujade, E. Grasland-Mongrain, A. Hertzog, J. Jouanneau, P. Chavrier, B. Ladoux, A. Buguin and P. Silberzan, *Proc Natl Acad Sci USA*, 2007, **104**, 15988–15993.
  - [13] S. R. K. Vedula, M. C. Leong, T. L. Lai, P. Hersen, A. J. Kabla, C. T. Lim and B. Ladoux, *Proc Natl Acad Sci U S A*, 2012, **109**, 12974–12979.
  - [14] O. Cochet-Escartin, J. Ranft, P. Silberzan and P. Marcq, *Biophys J*, 2014, **106**, 65–73.
  - [15] E. Bazellieres, V. Conte, A. Elosgui-Artola, X. Serra-Picamal, M. Bintanel-Morcillo, P. Roca-Cusachs, J. J. M. noz, M. Sales-Pardo, R. Guimerà and X. Trepat, *Nat Cell Biol*, 2015, **17**, 409–420.
  - [16] P. Lee and C. W. Wolgemuth, *PLoS Comput Biol*, 2011, **7**, e1002007.
  - [17] M. H. Köpf and L. M. Pismen, *Soft Matter*, 2012, **9**, 3727–3734.
  - [18] P. Recho, J. Ranft and P. Marcq, *Soft Matter*, 2016, **12**, 2381–2391.
  - [19] C. Blanch-Mercader, R. Vincent, E. Bazellieres, X. Serra-Picamal, X. Trepat and J. Casademunt, *Soft Matter*, 2017, **13**, 1235–1243.
  - [20] P. Lee and C. W. Wolgemuth, *Phys Rev E*, 2011, **83**, 061920.
  - [21] M. Köpf and L. Pismen, *Physica D*, 2013, **259**, 48–54.
  - [22] S. Banerjee, K. Utuje and M. Marchetti, *Phys Rev Lett*, 2015, **114**, 228101.
  - [23] C. Blanch-Mercader and J. Casademunt, *Soft Matter*, 2017, in press.
  - [24] S. Zehnder, M. K. Wiatt, J. M. Uruena, A. C. Dunn, W. G. Sawyer and T. E. Angelini, *Phys Rev E*, 2015, **92**, 032729.
  - [25] S. Zehnder, M. Suaris, M. M. Bellaire and T. E. Angelini, *Biophys J*, 2015, **108**, 247–250.
  - [26] B. Guirao, S. U. Rigaud, F. Bosveld, A. Bailles, J. López-Gay, S. Ishihara, K. Sugimura, F. Graner and Y. Bellaïche, *Elife*, 2015, **4**, e08519.
  - [27] S. Yabunaka and P. Marcq, *Phys Rev E*, 2017, in press.
  - [28] P. Chaikin and T. Lubensky, *Principles of Condensed Matter Physics*, Cambridge University Press, 2000.
  - [29] K. Kruse, J. Joanny, F. Jülicher, J. Prost and K. Sekimoto, *Eur Phys J E*, 2005, **16**, 5–16.
  - [30] M. C. Marchetti, J. F. Joanny, S. Ramaswamy, T. B. Liverpool, J. Prost, M. Rao and R. A. Simha, *Rev Mod Phys*, 2013, **85**, 1143–1189.
  - [31] L. Giomi and M. Marchetti, *Soft Matter*, 2012, **8**, 129–139.
  - [32] R. Mindlin, *Int J Solid Struct*, 1965, **1**, 417–438.
  - [33] P. Ciarletta, D. Ambrosi and G. Maugin, *J Mech Phys Solids*, 2012, **60**, 432–450.
  - [34] R. Ramaswamy and F. Jülicher, *Sci Rep*, 2016, **6**, 20838.
  - [35] P. Marcq, *Eur Phys J E*, 2014, **37**, 29.
  - [36] T. Das, K. Safferling, S. Rausch, N. Grabe, H. Boehm and J. P. Spatz, *Nat Cell Biol*, 2015, **17**, 276–287.
  - [37] R. Vincent, E. Bazellieres, C. Pérez-González, M. Uroz, X. Serra-Picamal and X. Trepat, *Phys Rev Lett*, 2015, **115**, 248103.
  - [38] T. B. Saw, A. Doostmohammadi, V. Nier, L. Kocgozlu, S. Thampi, Y. Toyama, P. Marcq, C. T. Lim, J. M. Yeomans and B. Ladoux, *Nature*, 2017, **544**, 212–216.